

This work was written as part of one of the author's official duties as an Employee of the United States Government and is therefore a work of the United States Government. In accordance with 17 U.S.C. 105, no copyright protection is available for such works under U.S. Law.

Public Domain Mark 1.0

<https://creativecommons.org/publicdomain/mark/1.0/>

Access to this work was provided by the University of Maryland, Baltimore County (UMBC) ScholarWorks@UMBC digital repository on the Maryland Shared Open Access (MD-SOAR) platform.

**Please provide feedback**

Please support the ScholarWorks@UMBC repository by emailing [scholarworks-group@umbc.edu](mailto:scholarworks-group@umbc.edu) and telling us what having access to this work means to you and why it's important to you. Thank you.



# Enhancing Triangulation of Interplanetary Type III Bursts through Wavevector Correction

Vratislav Krupar<sup>1,2</sup> , Oksana Kruparova<sup>1,2</sup> , Adam Szabo<sup>2</sup> , Rui F. Pinto<sup>3,4</sup> , Milan Maksimovic<sup>5</sup> , and Juan Carlos Martinez Oliveros<sup>6</sup>

<sup>1</sup> Goddard Planetary Heliophysics Institute, University of Maryland, Baltimore County, Baltimore, MD 21250, USA; [vratislav.krupar@nasa.gov](mailto:vratislav.krupar@nasa.gov)

<sup>2</sup> Heliospheric Physics Laboratory, Heliophysics Division, NASA Goddard Space Flight Center, Greenbelt, MD 20771, USA

<sup>3</sup> Institut de Recherche en Astrophysique et Planétologie, Université de Toulouse III (UPS), France

<sup>4</sup> Centre National de la Recherche Scientifique, UMR F-5277, Toulouse, France

<sup>5</sup> LESIA, Observatoire de Paris, Université PSL, CNRS, Sorbonne Université, Université de Paris, F-92195 Meudon, France

<sup>6</sup> Space Sciences Laboratory, University of California, Berkeley, CA 94720, USA

Received 2023 October 23; revised 2023 November 28; accepted 2023 December 11; published 2024 January 3

## Abstract

Interplanetary Type III bursts, generated by relativistic electron beams at solar flare reconnection sites, are explored through an investigation of 152 instances observed by the Solar Terrestrial Relations Observatory mission. This study reveals that the absolute values of the wavevector deviations from the Sun–spacecraft line are statistically 3.72 and 2.10 larger than predicted by the density model, assuming fundamental and harmonic emission, respectively. Through Monte Carlo simulations, we examine the impact of scattering by density inhomogeneities on the apparent locations of radio emissions in the interplanetary medium. The findings indicate that relative density fluctuations of 0.40 can account for the observed angular shift, a conclusion supported by the multiple flux-tube solar wind model, which confirms the presence of such magnitude of relative perpendicular density fluctuations in the solar wind. We propose a wavevector correction that incorporates this effect to enhance the triangulation of interplanetary Type III bursts, demonstrating that radio triangulation, with this correction, can reliably track electron beams in the interplanetary medium.

*Unified Astronomy Thesaurus concepts:* [Radio astronomy \(1338\)](#); [Radio bursts \(1339\)](#)

## 1. Introduction

Type III bursts, one of the most potent radio signals observed by space-borne and ground-based observatories, are generated by electron beams accelerated at solar flare reconnection sites, traveling through the corona and interplanetary medium (Wild 1950). These beams interact with background plasma, producing radio emissions at the electron plasma frequency,  $f_{pe}$ , and its first harmonic,  $2f_{pe}$ , via the plasma emission mechanism (Ginzburg & Zhelezniakov 1958). While distinguishable at shorter wavelengths, the fundamental and harmonic components become nearly indistinguishable at longer wavelengths in the interplanetary medium (Stewart 1974; Reiner et al. 1998).

Type III radio bursts serve as vital indicators of electron beam activity in the solar corona and interplanetary space (Reid 2020). Coronal Type III bursts, observed at high frequencies by ground-based radio telescopes such as LOW Frequency ARray (van Haarlem et al. 2013) and Murchison Widefield Array (Lonsdale et al. 2009), trace electron transport close to their acceleration region in the corona. These bursts provide key insights into the initial characteristics of the electron beams. On the other hand, interplanetary Type III emissions are detected at lower frequencies by spacecraft, offering crucial diagnostics for electron beams that have journeyed further into interplanetary space and undergone more extensive propagation effects (Dulk 2000). These interplanetary emissions are essential for understanding the connectivity of the solar wind’s magnetic field and for space

weather studies, especially after accounting for radio propagation effects (Kontar et al. 2017).

Adjustments to coronal density models (e.g., Newkirk 1961; Saito et al. 1970; Vršnak et al. 2004) are often required for interpreting coronal Type III bursts due to the complex density structures within the corona (Magdalenic et al. 2014). These adjustments help in accurately converting frequency observations to radial distances. In contrast, for interplanetary Type III bursts in the frequency range between 1 MHz and 100 kHz, density models such as those from Leblanc et al. (1998) and Sittler & Guhathakurta (1999) are typically more reliable and do not necessitate significant modifications, unless the bursts originate in overdense regions of the solar wind. This distinction highlights the relative simplicity of interpreting interplanetary Type III bursts as compared to their coronal counterparts. Despite their detectability across a wide longitudinal range, the apparent radio sources of Type III bursts are situated at notably larger radial distances than electron density models predict and can envelop the entire inner heliosphere (Bonnin et al. 2008; Reiner et al. 2009; Krupar et al. 2014a). These properties, attributed to the scattering of radio waves by electron density inhomogeneities, can be explored through geometric optics methods and Monte Carlo simulations (Hollweg 1968; Steinberg et al. 1984).

Thejappa et al. (2007) pioneered a Monte Carlo simulation code, meticulously exploring the impact of refraction and scattering attributed to the spatial variation of solar wind density and random density fluctuations, respectively, on the directivities, temporal profiles, and apparent source characteristics of interplanetary solar radio bursts. Subsequently, Krupar et al. (2018) juxtaposed decay times of Type III bursts, as observed by the Solar TERrestrial RELations Observatory



Original content from this work may be used under the terms of the [Creative Commons Attribution 4.0 licence](#). Any further distribution of this work must maintain attribution to the author(s) and the title of the work, journal citation and DOI.

(STEREO), with Monte Carlo simulations, leveraging the foundational work of Thejappa et al. (2007). This comparison illuminated that the emblematic exponential decay profile could be deciphered through the scattering of the fundamental component between the source and observer, estimating the relative electron density fluctuations to oscillate between 0.06 and 0.07 at radial distances spanning 8–45 solar radii ( $1 R_{\odot} = 695,500 \text{ km}$ ).

Recently, Krupar et al. (2020) conducted a detailed analysis of 30 Type III bursts detected by the Parker Solar Probe (PSP), extracting burst decay times,  $\tau_d$ , across the 1 to 10 MHz frequency range, leveraging the unparalleled temporal resolution of PSP. Through a comparative approach involving PSP observations and Monte Carlo simulations, Krupar et al. (2020) projected relative density fluctuations,  $\epsilon$ , at the effective turbulence scale length, to vary from 0.22 to 0.09 at radial distances spanning 2.5 to 14  $R_{\odot}$ . Furthermore, Krupar et al. (2020) computed in situ relative density fluctuations,  $\epsilon$ , measured by PSP at a radial distance of 35.7  $R_{\odot}$  during its first and second perihelions, revealing values of 0.07 and 0.06, respectively. These findings align well with previous predictions by Krupar et al. (2018) using STEREO ( $\epsilon = 0.06\text{--}0.07$ ), obtained through remote measurements of radio sources generated at this radial distance.

Here, we primarily scrutinize radio measurements procured by the STEREO mission, which operates in a circumsolar orbit approximately 1 au ( $1 \text{ au} = 149,598,000 \text{ km}$ ) from the Sun. Each spacecraft in the mission is equipped with the STEREO/Waves/High Frequency Receiver (125 kHz–16 MHz), which meticulously records electric field fluctuations utilizing three monopole antennas (Bougeret et al. 2008). Our analysis is centered on radio observations of Type III bursts, specifically within the frequency range of 125–975 kHz. This encompasses 17 frequency channels, each with a bandwidth of 25 kHz, where dependable direction-finding data are accessible (Krupar et al. 2012).

We undertake a comprehensive examination of Type III solar radio bursts, with a primary focus on quantifying the deviations in observed wavevector directions from those predicted by electron density models (Section 2.1). Rather than introducing a new model, our approach centers on a detailed analysis of these deviations, revealing significant insights into the propagation dynamics of Type III bursts. Using Monte Carlo simulations, we meticulously evaluate the impact of scattering by density inhomogeneities on wavevector directions, thus enhancing our understanding of burst propagation in the interplanetary medium (Section 2.2). Further, we analyze relative density fluctuations within the solar wind, drawing on data and predictions from the multiple flux-tube solar wind (MULTI-VP) model to provide context and depth to our findings (Section 2.3). The culmination of our research is the introduction of a novel wavevector correction method. Through detailed analysis of a specific Type III burst and a comprehensive statistical survey, we aim to significantly improve the accuracy and reliability of radio triangulation methods (Section 2.4). This aspect of our work is particularly innovative, as it presents a new way to refine radio triangulation in space weather studies. Overall, our investigation endeavors to provide a deeper, more nuanced understanding of the dynamics and interactions of Type III bursts within the interplanetary medium, emphasizing the importance

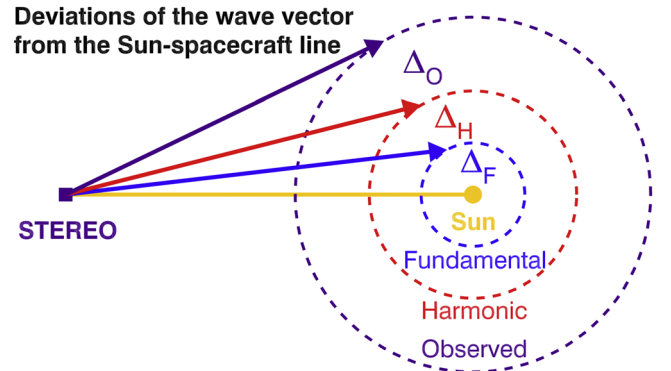


**Figure 1.** Illustration of wavevector deviations from the Sun–spacecraft line, contrasting observed deviations (in purple) with modeled deviations for fundamental and harmonic emissions (in blue and red, respectively). Dashed circles indicate observed and modeled radio emission altitudes.

of precise measurement and analysis techniques in advancing our knowledge of solar phenomena.

## 2. Observation and Analysis

### 2.1. Wavevector Directions

Despite decades of regular measurements of interplanetary solar radio emissions, a comprehensive model elucidating their expansive apparent source sizes, broad visibility, and differentiation between fundamental and harmonic components remains elusive. Specifically, the wavevector directions of solar radio bursts point notably further from the Sun–spacecraft line than predicted by average density models, implying an apparent shift of observed radio sources away from the Sun (Figure 1).

A statistical analysis was conducted on 152 Type III radio bursts observed by STEREO from 2007 May to 2013 February, a data set previously utilized for studying radio source locations, radio flux frequency variations, and decay times (Krupar et al. 2014a, 2014b, 2018). Employing the density model of Sittler & Guhathakurta (1999), STEREO frequencies (125 kHz–975 kHz) were converted into radial distances, assuming fundamental and harmonic emissions (Figure 2(a)). Radio sources were uniformly distributed on a circle with a radius derived from the density model (Figure 1), and median values of modeled wavevector deviations  $\Delta_F$  and  $\Delta_H$  were calculated (Figure 2(b)). The modeled deviations were adjusted to average radial distances of STEREO-A (red, 0.96 au) and STEREO-B (blue, 1.06 au) over the entire period, varying between  $1^\circ$  and  $20^\circ$  within this frequency range.

In our analysis, observed wavevector deviations  $\Delta$  from STEREO-A and STEREO-B exhibited a significant range, spanning approximately  $6^\circ\text{--}60^\circ$ . These deviations are markedly greater than those predicted by existing models, as depicted in Figure 2(b). To quantify this disparity, we calculated the ratio  $\Xi$  between observed and modeled deviations, as shown in Figures 2(c) and (d). This calculation revealed that the observed deviations for the fundamental and harmonic emissions were statistically  $\Xi_F = 3.72$  and  $\Xi_H = 2.10$ , respectively, within the 350 kHz to 1 MHz frequency range. Notably, these parameters demonstrated almost frequency-independent characteristics across this spectrum.

This variation magnitude, specifically the factors of 3.72 and 2.10, significantly surpasses the expected accuracy of prevalent density models, such as the one proposed by

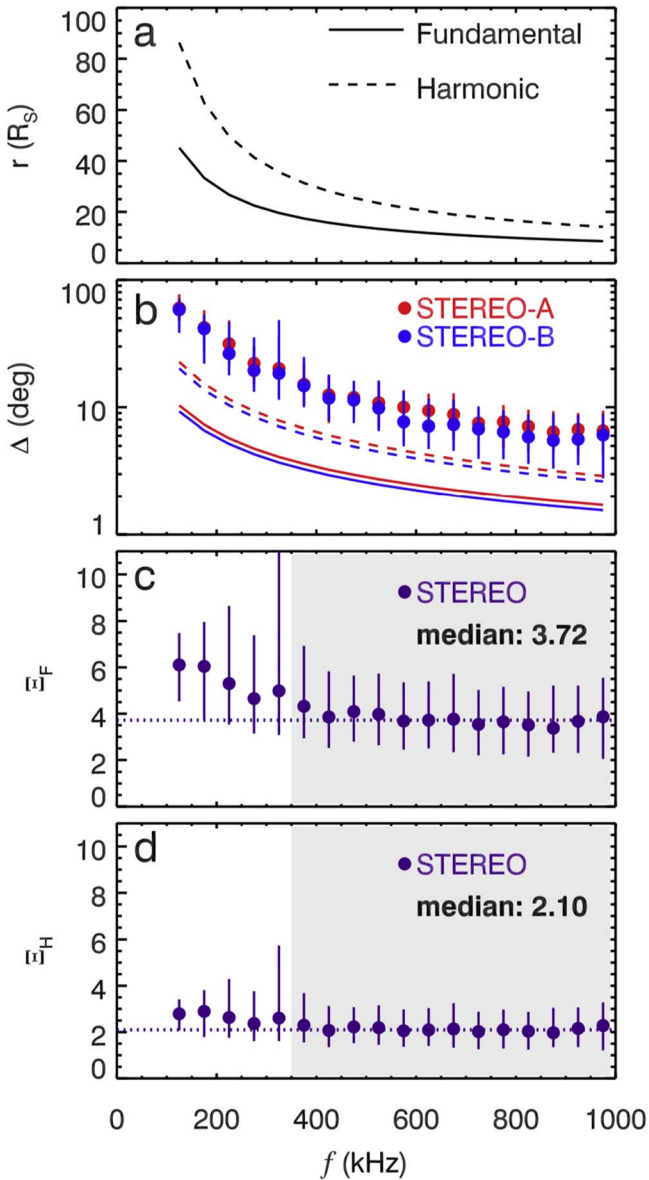


**Figure 2.** Statistical analysis of 152 Type III bursts, featuring (a) the density model from Sittler & Guhathakurta (1999) for fundamental and harmonic emissions, (b) observed wavevector deviations vs. frequency for STEREO-A and STEREO-B, and (c) and (d) relative deviations for fundamental and harmonic emissions, with dotted lines representing median values between 350 kHz and 1 MHz.

Sittler & Guhathakurta (1999). Although other models, like that of Leblanc et al. (1998), yield similar electron densities within our frequency range, the observed deviations still stand out as substantially more pronounced. Previous statistical studies by Leblanc et al. (1974) and Leblanc & de La Noe (1977) have discounted the hypothesis that Type III bursts are predominantly generated in denser plasma regions. Thus, our observations suggest that Type III bursts occur statistically farther from the Sun than average density models predict. Such a discrepancy in the observed wavevector deviations, significantly exceeding the variations among different density models, underscores the necessity of an alternative explanation. The following section delves into Monte Carlo simulations, which offer a compelling insight into these discrepancies and provide a robust framework for understanding the observed phenomena.

## 2.2. Monte Carlo Simulations

In an effort to interpret the acquired values of  $\Xi$  and to delve deeper into the intricate dynamics of Type III bursts, we executed Monte Carlo simulations. These simulations were aimed at quantifying the influence of scattering by density inhomogeneities on the wavevector directions of these bursts, as illustrated in Figure 3. The methodology employed in the simulations adheres closely to that of Krupar et al. (2018), incorporating several simplifications for computational feasibility and clarity. These simplifications include (1) the assumption of an isotropic point source, (2) the utilization of a spherically symmetric solar wind electron density model, (3) the application of a power-law distribution for electron density fluctuations with a spectral index that aligns with Kolmogorov turbulence theory, and (4) the assumption of a constant isotropic relative electron density fluctuation, denoted as  $\epsilon = \langle \delta n \rangle / \langle n \rangle$ , within the solar wind.

Figure 3 provides a visual representation of the outcomes of the simulations, illustrating that the scattering effect is notably more pronounced for the fundamental component and that relative deviations increase with  $\epsilon$ . This is particularly insightful as it provides a quantitative framework to understand the scattering phenomena in the context of Type III solar radio bursts.

Figure 4 presents a detailed overview of the results derived from the Monte Carlo simulations, showcasing outcomes for 11 distinct levels of density fluctuations across the 17 frequency channels that were analyzed by the STEREO spacecraft. The findings suggest that a relative density fluctuation level of  $\epsilon = 0.40$  is requisite to account for the observed relative deviations of wavevector directions—3.72 and 2.10 for the fundamental and harmonic emission, respectively.

The apparent discrepancy between the density fluctuations obtained by comparing Monte Carlo simulations with Type III burst decay times ( $\epsilon = 0.06$ ) and the deviations of wavevector directions ( $\epsilon = 0.40$ ) may be ascribed to the anisotropic nature of density turbulence in the solar wind. It's noteworthy that the Monte Carlo simulation code presumes the existence of isotropic density fluctuations exclusively. This assumption, while simplifying the computational model, may not fully encapsulate the complex, anisotropic turbulence characteristics of the solar wind, thereby providing a pathway for future research and model refinement in this domain.

In a recent advancement, Kontar et al. (2019) unveiled a 3D stochastic model that encapsulates the radio wave propagation process, incorporating anisotropic electron density fluctuations. When juxtaposed with observations of solar radio bursts, particularly those utilizing ground-based instruments, which observe at higher frequencies than their space-based counterparts, the simulations underscored a necessity for predominantly perpendicular density fluctuations within the solar corona. Specifically, an anisotropy factor of approximately 0.3 was requisite for sources observed in the vicinity of 30 MHz.

In a study conducted by DeForest et al. (2018), the fine-scale structure of the outer corona was meticulously examined, utilizing a unique data set obtained from a deep-exposure campaign using the STEREO-A/SECCHI/COR2 instrument. The researchers identified propagating blobs, which exhibited a distinct anisotropic structure. Specifically, the smallest spatial scales in the radial direction were found to be elongated compared to the azimuthal direction of the surrounding striae.



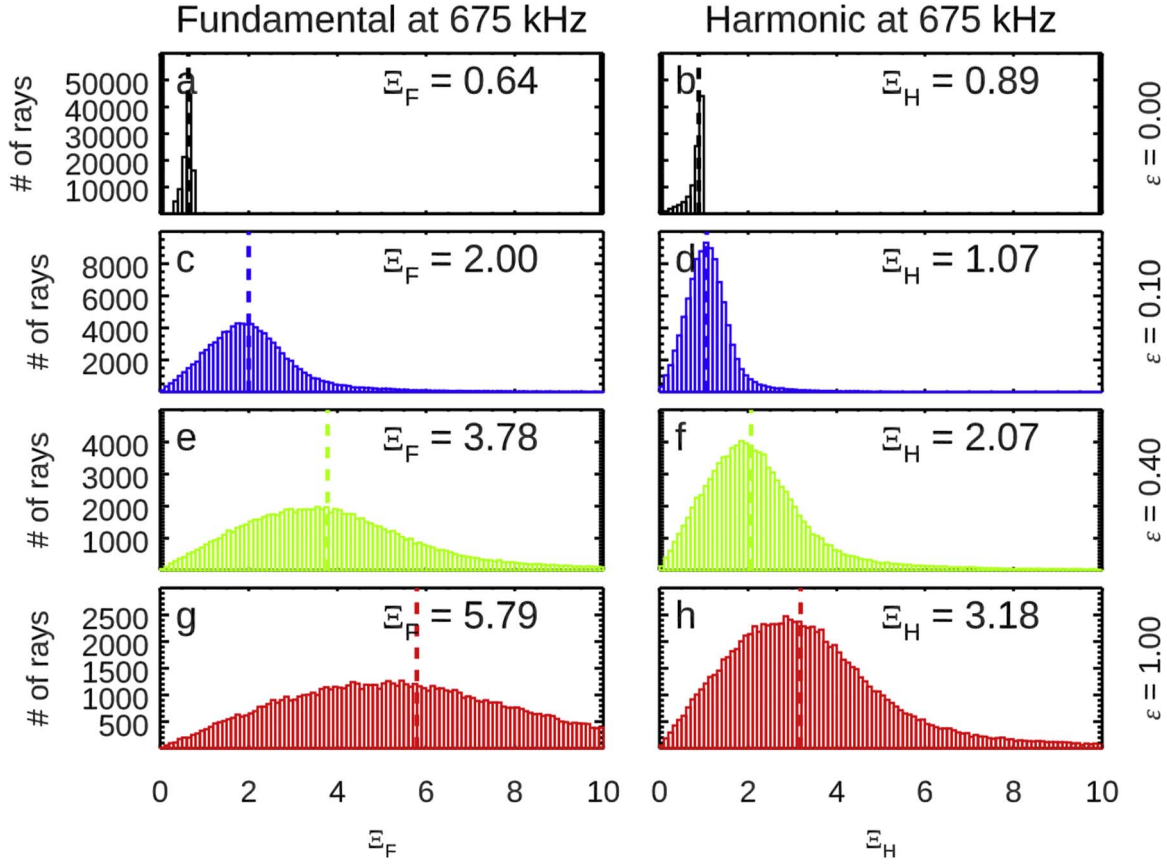


**Figure 3.** Monte Carlo simulation results, depicting modeled relative deviations  $\Xi_F$  and  $\Xi_H$  across four levels of relative density fluctuations, assuming fundamental and harmonic emission at 675 kHz. Dashed lines indicate median values.

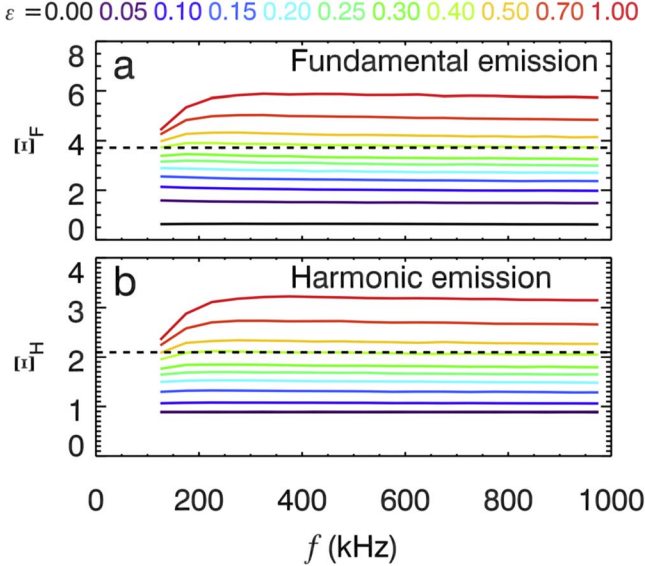


**Figure 4.** Modeled relative deviations  $\Xi_F$  and  $\Xi_H$  vs. frequency for 11 levels of relative density fluctuations, assuming fundamental and harmonic emission. Dashed lines denote factors 3.72 and 2.10 extracted from Figure 2, facilitating a comparative analysis across fluctuation levels.

This implies that the deep-exposure observations of the outer corona demonstrated a significant discrepancy between perpendicular and parallel anisotropy, with the former being considerably larger. This pivotal finding not only provides profound insights into the dynamics and structural composition

of the outer corona but also potentially influences our understanding of the solar wind and its interactions with the interplanetary medium, thereby opening new avenues for further research and exploration in this domain.

### 2.3. MULTI-VP Model Analysis

We utilized the MULTI-VP (Pinto & Rouillard 2017) model to investigate relative density fluctuations across 51 Carrington rotations (Figure 5). The MULTI-VP model is adept at computing the three-dimensional structure of the solar wind, encompassing the chromosphere, the transition region, the corona, and the lower heliosphere. It achieves this by calculating wind profiles along open magnetic field lines, thus sampling the entire solar atmosphere. The radial domain of these calculations extends from the photosphere up to approximately  $30 R_S$ , with the solutions based on a sophisticated numerical scheme adaptable to various flux-tube geometries.

Our analysis revealed that perpendicular relative density fluctuations, denoted as  $\epsilon_{\perp}$ , varied between 0.22 and 0.37 over radial distances corresponding to radio sources generated between 1 MHz and 350 kHz. This range is highlighted in Figure 5(b). Notably, these fluctuations remained nearly constant between  $20 R_S$  and  $30 R_S$ . In contrast, parallel density fluctuations,  $\epsilon_{\parallel}$ , showed a decreasing trend, adhering to a power law of  $-1$ . This notable difference between perpendicular and parallel fluctuations provides an intriguing area for future research, potentially revealing new insights into the underlying physical processes and their impact on solar wind dynamics.

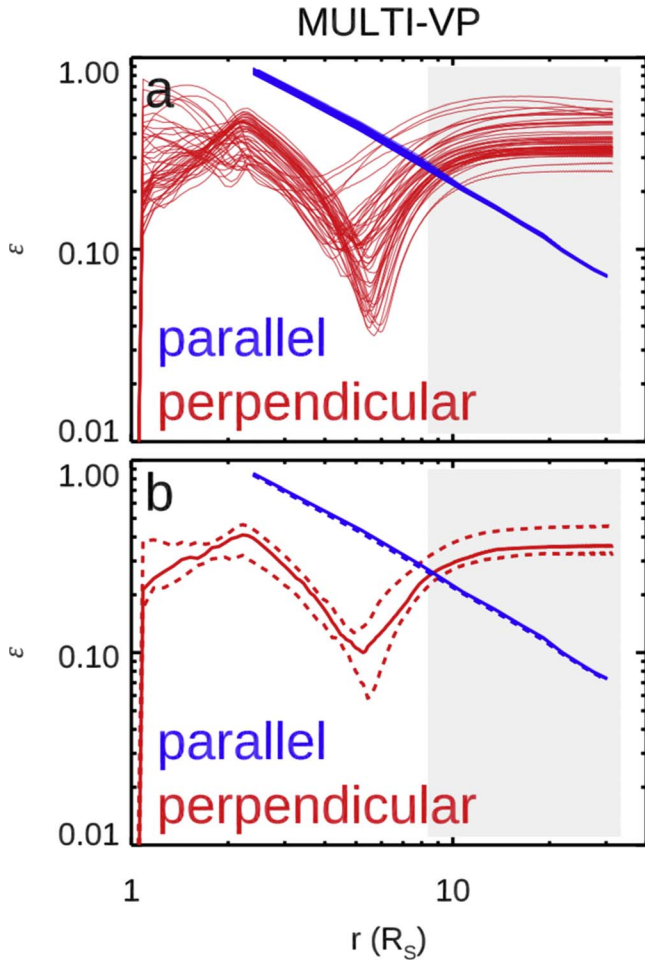


**Figure 5.** Outcomes derived from the MULTI-VP model, encompassing 51 Carrington rotations (2007 March 31—2017 December 31). Displaying (a) both parallel and perpendicular relative density fluctuations for each individual rotation, and (b) median values, complemented by error bars representing the 25th/75th percentiles, extracted from the data presented in panel (a), thereby offering a nuanced perspective into the fluctuations’ variability and stability over time.

Summarizing our findings from Monte Carlo simulations of radio wave propagation, we conclude that density fluctuations of approximately 40% are necessary to account for the observed relative deviations in wavevector directions:  $\Xi_F = 3.72$  and  $\Xi_H = 2.10$  for fundamental and harmonic emissions, respectively. This level of fluctuation is consistent with the predictions of the MULTI-VP model, which estimates solar wind fluctuations to be around 0.22–0.37 during the period when Type III bursts were observed. This correlation not only validates our simulation approach but also highlights the MULTI-VP model’s accuracy in reflecting the dynamic nature of solar wind fluctuations.

#### 2.4. Wavevector Correction

In this section, we delve into a comprehensive analysis of a Type III burst that transpired on 2010 January 10, during a period when the STEREO spacecraft were separated by 133° (refer to Figure 6). The electron beam speeds, ascertained through a meticulous radio triangulation analysis, were notably larger than those derived from a frequency drift. Consequently, we introduced a wavevector correction, which effectively reduced its deviation from the Sun–spacecraft line by factors of

3.72 and 2.10 for the fundamental and harmonic emission, respectively. This adjustment facilitated a commendable agreement between the radio triangulation utilizing the corrected directions and the frequency drift technique, thereby enhancing the reliability and accuracy of our findings.

Our exploration extended to 23 Type III bursts, which were observed by the two STEREO spacecraft and exhibited suitable parameters conducive for a thorough radio triangulation analysis (see Figure 7). Through this investigation, we demonstrated that employing the radio triangulation technique, especially when utilizing the corrected directions, yields reasonable and scientifically robust results on a statistical basis. This implies that radio sources of Type III bursts can be reliably utilized to track electron beams traversing the interplanetary medium, providing invaluable insights into their propagation characteristics and interactions with the surrounding medium.

Moreover, our analysis not only sheds light on the specific characteristics of the Type III bursts but also paves the way for future research aimed at unraveling the intricate dynamics and mechanisms underlying these fascinating solar phenomena. The methodologies and findings presented herein could potentially serve as a foundation for subsequent studies, enabling researchers to further probe into the mysteries of Type III bursts and their role in shaping the interplanetary medium. This, in turn, could enhance our understanding of solar wind dynamics, electron beam propagation, and the overall impact of solar activity on the heliosphere, thereby contributing to the broader field of solar-terrestrial physics.

### 3. Conclusion

We have delved into the intricate dynamics of Type III solar radio bursts, focusing particularly on quantifying the deviations between observed and modeled wavevector directions. Our comprehensive analysis of 152 Type III radio bursts observed by STEREO has revealed significant disparities between these observed deviations and those predicted by electron density models. By determining the ratios  $\Xi_F$  and  $\Xi_H$ , we have established a framework for understanding scattering phenomena in Type III solar radio bursts.

Our findings highlight the role of anisotropic turbulence in understanding both the long decay times and the wavevector variations observed in these bursts. The Monte Carlo simulations, while based on a simplified model, have shed light on the influence of density inhomogeneities on the wavevector directions of Type III bursts. The necessity for density fluctuations of about 40% to explain the observed deviations aligns with the predictions from the MULTI-VP model, emphasizing the model’s accuracy in solar wind dynamics representation.

The introduction of a wavevector correction method in this study marks a significant innovation in solar physics. This correction not only enhances the accuracy of radio triangulation for tracking electron beams in the interplanetary medium but also has the potential to improve our capability to trace magnetic field lines associated with Type III bursts. Furthermore, when applied to Type II bursts, this method could significantly advance our ability to track coronal mass ejections. Such advancements underscore the potential of our method in enhancing our understanding of solar phenomena.

In conclusion, our study provides foundational insights into the structural composition and dynamics of Type III bursts and the solar wind, highlighting the pivotal role of anisotropic

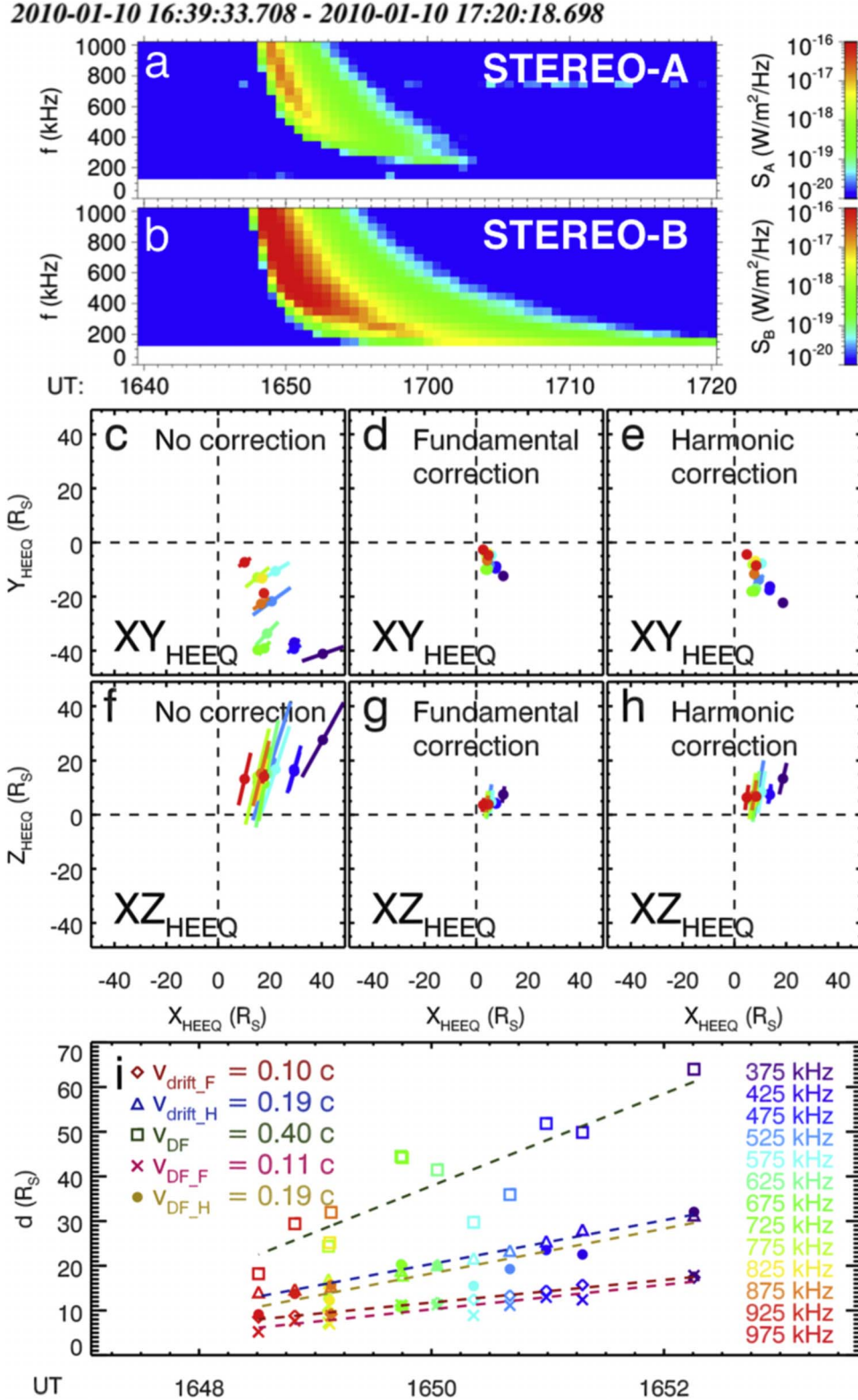


**Figure 6.** Radio measurements of the 2010 January 10 Type III burst. (a) and (b) Radio flux density  $S$  for STEREO-A and STEREO-B. (c)–(h) Triangulated radio sources without the correction (left), with the fundamental correction (middle), and with the harmonic correction (right) in the  $XY_{\text{HEEQ}}$  (top) and  $XZ_{\text{HEEQ}}$  (bottom) planes. Colors denote frequency (panel (i) right). Segment lines indicate the accuracy of the triangulation. (i) Height–time profiles retrieved from the density model (the fundamental emission: diamonds; the harmonic emission: triangles), from the radio triangulation without the correction (squares), and from the radio triangulation with the fundamental (crosses) and harmonic (circles) correction. Dashed lines are linear fits. Obtained speeds are in the top left corner.

turbulence. It opens new avenues for further research and exploration, paving the way for future studies to build upon our methodologies and findings. These future endeavors may

uncover new insights into the physical phenomena governing Type III bursts and their impact on the heliosphere, contributing substantially to the field of solar-terrestrial physics.



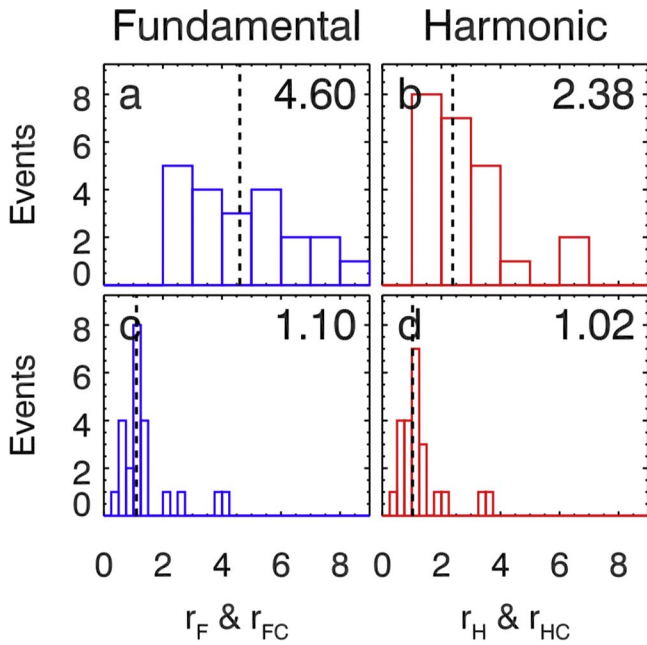


**Figure 7.** Results derived from a statistical survey of 23 Type III bursts, showcasing histograms of ratios between electron beam speeds retrieved by radio triangulation without (panels (a) and (b)) and with the correction (panels (c) and (d)), and by the density model for fundamental and harmonic emission. Dashed lines represent median values, offering a statistical insight into the electron beam speeds and their distribution across the analyzed bursts.

### Acknowledgments

The authors would like to thank the many individuals and institutions who contributed to making STEREO possible. V.K. was supported by the STEREO/Waves and Wind/Waves projects, and by the NASA grant 19-HSR-19\2-0143. Radio data are publicly available at <http://spdf.gsfc.nasa.gov/>.

### ORCID iDs

Vratislav Krupar <https://orcid.org/0000-0001-6185-3945>  
Oksana Kruparova <https://orcid.org/0000-0002-1122-6422>

Adam Szabo <https://orcid.org/0000-0003-3255-9071>  
Rui F. Pinto <https://orcid.org/0000-0001-8247-7168>  
Milan Maksimovic <https://orcid.org/0000-0001-6172-5062>  
Juan Carlos Martinez Oliveros <https://orcid.org/0000-0002-2587-1342>

### References

- Bonnin, X., Hoang, S., & Maksimovic, M. 2008, *A&A*, **489**, 419  
Bougeret, J. L., Goetz, K., Kaiser, M. L., et al. 2008, *SSRv*, **136**, 487  
DeForest, C. E., Howard, R. A., Velli, M., Viall, N., & Vourlidas, A. 2018, *ApJ*, **862**, 18  
Dulk, G. A. 2000, *GMS*, **119**, 115  
Ginzburg, V. L., & Zhelezniakov, V. V. 1958, *SvA*, **2**, 653  
Hollweg, J. V. 1968, *AJ*, **73**, 972  
Kontar, E. P., Chen, X., Chrysaphi, N., et al. 2019, *ApJ*, **884**, 122  
Kontar, E. P., Yu, S., Kuznetsov, A. A., et al. 2017, *NatCo*, **8**, 1515  
Krupar, V., Maksimovic, M., Kontar, E. P., et al. 2018, *ApJ*, **857**, 82  
Krupar, V., Maksimovic, M., Santolik, O., Cecconi, B., & Kruparova, O. 2014a, *SoPh*, **289**, 4633  
Krupar, V., Maksimovic, M., Santolik, O., et al. 2014b, *SoPh*, **289**, 3121  
Krupar, V., Santolik, O., Cecconi, B., et al. 2012, *JGRA*, **117**, A06101  
Krupar, V., Szabo, A., Maksimovic, M., et al. 2020, *ApJS*, **246**, 57  
Leblanc, Y., & de La Noe, J. 1977, *SoPh*, **52**, 133  
Leblanc, Y., Dulk, G. A., & Bougeret, J.-L. 1998, *SoPh*, **183**, 165  
Leblanc, Y., Kuiper, T. B. H., & Hansen, S. F. 1974, *SoPh*, **37**, 215  
Lonsdale, C. J., Cappallo, R. J., Morales, M. F., et al. 2009, in *IEEE The Murchison Widefield Array: Design Overview* (Piscataway, NJ: IEEE), 1497  
Magdalenic, J., Marqué, C., Krupar, V., et al. 2014, *ApJ*, **791**, 115  
Newkirk, Gordon, J. 1961, *ApJ*, **133**, 983  
Pinto, R. F., & Rouillard, A. P. 2017, *ApJ*, **838**, 89  
Reid, H. A. S. 2020, *FrASS*, **7**, 56  
Reiner, M. J., Fainberg, J., Kaiser, M. L., & Stone, R. G. 1998, *JGR*, **103**, 1923  
Reiner, M. J., Goetz, K., Fainberg, J., et al. 2009, *SoPh*, **259**, 255  
Saito, K., Makita, M., Nishi, K., & Hata, S. 1970, *AnTok*, **12**, 51  
Sittler, Edward C., Jr., & Guhathakurta, M. 1999, *ApJ*, **523**, 812  
Steinberg, J. L., Hoang, S., Lecacheux, A., Aubier, M. G., & Dulk, G. A. 1984, *A&A*, **140**, 39  
Stewart, R. T. 1974, *SoPh*, **39**, 451  
Thejappa, G., MacDowall, R. J., & Kaiser, M. L. 2007, *ApJ*, **671**, 894  
van Haarlem, M. P., Wise, M. W., Gunst, A. W., et al. 2013, *A&A*, **556**, A2  
Vršnak, B., Magdalenic, J., & Zlobec, P. 2004, *A&A*, **413**, 753  
Wild, J. P. 1950, *AuSRA*, **3**, 541